Photodissociation Dynamics of Phenol†

Chien-Ming Tseng,[‡,§] Yuan T. Lee,[‡,§] Ming-Fu Lin,[‡] Chi-Kung Ni,*[,‡,£] Suet-Yi Liu,[‡,#] Yuan-Pern Lee,*[,‡,#] Z. F. Xu,[¶] and M. C. Lin*[,#,¶]

Institute of Atomic and Molecular Sciences, Academia Sinica, P. O. Box 23-166, Taipei 10617, Taiwan, Department of Chemistry, National Taiwan University, Taipei 10617, Taiwan, Department of Chemistry, National Tsing Hua University, Hsinchu, Taiwan, Department of Applied Chemistry and Institute of Molecular Science, National Chiao Tung University, Hsinchu 30010, Taiwan, and Department of Chemistry, Emory University, Atlanta, Georgia 30322

Received: April 29, 2007; In Final Form: July 24, 2007

The photodissociation of phenol at 193 and 248 nm was studied using multimass ion-imaging techniques and step-scan time-resolved Fourier-transform spectroscopy. The major dissociation channels at 193 nm include cleavage of the OH bond, elimination of CO, and elimination of H_2O. Only the former two channels are observed at 248 nm. The translational energy distribution shows that H-atom elimination occurs in both the electronically excited and ground states, but elimination of CO or H_2O occurs in the electronic ground state. Rotationally resolved emission spectra of CO ($1 \le v \le 4$) in the spectral region of 1860−2330 cm^{-1} were detected upon photolysis at 193 nm. After a correction for rotational quenching, CO ($v \le 4$) shows a nascent rotational temperature of ∼4600 K. The observed vibrational distribution of $(v = 1)/(v = 2)/(v = 3)/(v = 4) = 64.3/22.2/9.1/4.4$ corresponds to a vibrational temperature of 3350 ± 20 K. An average rotational energy of 6.9 ± 0.7 kcal mol^{-1} and vibrational energy of 3.8 ± 0.7 kcal mol^{-1} are observed for the CO product. The dissociation channels, translational energy distributions of the photofragment, and vibrational and rotational energies of product CO are consistent with potential energy surfaces from quantum chemical calculations and the branching ratios from an RRKM calculation.

1. Introduction

Because of its antioxidative properties, the photophysics and photochemistry of phenol (C_6H_5OH) are of great interest to various fields of science and technology. The following paths of a phenol molecule excited to its first excited singlet state (S_1) in the condensed phase have been suggested[1,2]

$$C_6H_5OH\ (S_1) \rightarrow C_6H_5OH\ (S_0) + h\nu \text{ (fluorescence)}$$
$$\rightarrow C_6H_5OH\ (S_0) + E \text{ (internal conversion)}$$
$$\rightarrow C_6H_5OH\ (T_1) + E \text{ (intersystem crossing)}$$
$$\rightarrow C_6H_5O + H \text{ (photodissociation)}$$
$$\rightarrow [C_6H_5OH^+\cdots e^-]_{aq} \rightarrow C_6H_5O + H \text{ (photoionization in aqueous solution at high pH)}$$

Laser flash photolysis of phenol at 253 nm with detection by both picosecond and nanosecond emission and absorption has been performed to reveal information of the deactivation channels of the first excited singlet state.[1] The fluorescence lifetime on phenol near 295 K was found to be a few nanoseconds. The photodissociation yield of phenol was found to be ∼0.1, nearly independent of solvent, but the quantum yield of intersystem crossing varied between 0.2 and 0.3, with smaller values in nonpolar media and larger ones in polar media. No dissociation occurred upon excitation at 266 nm in the condensed phase because the photon energy was insufficient for direct fission of the OH bond.

Most research on gaseous phenol in its S_1 state has been focused on its spectroscopy. Phenol and various phenol-containing clusters have been investigated. For instance, phenol−ammonia clusters have been studied extensively by fluorescence and multiphoton ionization.[3−10] Accordingly, this system was considered to be a model system to investigate proton-transfer reactions in the excited state in molecular clusters, but further experiments indicate that, instead of proton transfer on the excited-state surface, transfer of a H atom occurs on the S_1 surface.[11−15] Quantum chemical calculations show that an excited singlet state of $\pi\sigma^*$ character, being repulsive with respect to stretching of the OH bond, intersects the bound state $S_1(\pi\pi^*)$ near an energy level of 5 eV (∼248 nm).[16−18] Hydrogen transfer in phenol−ammonia clusters was explained as predissociation of the $S_1(\pi\pi^*)$ state via this low-lying $\pi\sigma^*$ state. The role of a repulsive $\pi\sigma^*$ state in dissociation is consistent with the large release of translational energy in the channel involving H-atom elimination observed in the photodissociation of phenol in a molecular beam.[19,20]

The excitation of phenol to the S_2 excited state has also been investigated, but varied conclusions have been derived. For phenol in solution, Dellonte et al.[21,22] studied the temperature dependence of internal conversion (IC) from S_2 to S_1, competing electron-solvation processes, and the cleavage of the OH bond

† Part of the "Sheng Hsien Lin Festschrift".

* To whom correspondence should be addressed. E-mail: ckni@po.iams.sinica.edu.tw (C.-K.N.); yplee@mail.nctu.edu.tw (Y.-P.L.); chemmcl@emory.edu (M.C.L.).

‡ Academia Sinica.

§ National Taiwan University.

£ National Tsing Hua University.

National Chiao Tung University.

¶ Emory University.

10.1021/jp073282z CCC: $37.00 © 2007 American Chemical Society
Published on Web 08/10/2007

by observing fluorescence quantum yields. A rate coefficient of $k_{IC} = 3 \times 10^{11}$ s^{-1} was determined, and the intersystem crossing (ISC) to a dissociative triplet state with $k_{ISC} = 7 \times 10^{11}$ s^{-1} was suggested. In contrast, time-resolved photoelectron spectra after two-photon ionization showed that the internal conversion from S_2 to S_1 is the dominant pathway, with a time scale in the range of 150−350 fs.[23] It also showed no evidence of competing processes, such as intersystem crossing to a triplet surface, as previously postulated, or an intramolecular vibrational energy redistribution (IVR) process within S_2. Absorption spectra of the gaseous phenoxyl radical were recorded upon excitation of phenol to the S_2 state at 193 nm.[24] The dissociation was explained in terms of predissociation. Photodissociation of phenol at 193 in a condensed phase studied by Fourier-transform electron paramagnetic resonance and transient absorption spectroscopy also produced cleavage of the OH bond.[2]

In this work, we investigated the photodissociation of gaseous phenol at 193 and 248 nm. Distributions of the translational energy of photofragments and of the vibrational and rotational states of CO were measured. We characterized the potential energy hypersurfaces with quantum chemical calculations and evaluated the branching ratios for various dissociation channels with Rice−Ramsperger−Kassel−Marcus (RRKM) calculations.

2. Experiments Section

A. Multimass Ion Imaging. As the experimental techniques have been described in detail,[25−27] only a brief description is given here. Phenol vapor was prepared on flowing ultrapure He (or Ne) at a pressure of 400 Torr through a reservoir containing solid phenol at 323 K. The phenol/He mixture was then expanded through a pulsed nozzle (diameter 500 μm) maintained at 353 K to form a molecular beam. Molecules in that beam were photodissociated with a pulsed UV laser, followed by ionization with a pulsed VUV laser at 118 nm; a pulsed electric field served to extract the ions into a mass spectrometer. At the exit port of the mass spectrometer, a two-dimensional ion detector was used to detect the ion positions and intensity distribution. In this two-dimensional detector, one axis pertained to the recoil velocity and the other to the mass.

B. Step-Scan Time-Resolved Fourier-Transform Spectroscopy. The apparatus employed to obtain step-scan time-resolved Fourier-transform spectra (TR-FTS) has been described;[28−30] only a brief summary is given here. A lens mildly focused the photolysis beam from an ArF laser at 193 nm (Gam Laser, EX100H/60) to ~6 × 15 mm^2 at the reaction center with a fluence of ~24 mJ cm^{-2}. A filter passing 1860−2330 cm^{-1} was employed. We used an InSb detector with a rise time of 0.22 μs, of which the transient signal was preamplified with a gain factor of 8×10^5 V A^{-1}, followed by amplification by a factor of 100 (Stanford Research Systems, SRS560, 1 MHz) before being digitized with an external data acquisition board (PAD1232, 12-bit ADC) at 50 ns resolution. Data were typically averaged over 27 laser pulses at each scan step; after undersampling, 3781 scan steps were performed to yield an interferogram, resulting in a spectrum with a resolution of 0.3 cm^{-1}. To improve the ratio of signal-to-noise (S/N) of the spectrum, 10−30 consecutive time-resolved spectra were subsequently summed to yield a satisfactory spectrum representing emission at intervals of 0.2−1.2 μs.

C_6H_5OH was injected into the vacuum chamber as a diffusive beam through a slit-shaped inlet. The sample was heated to ~318 K; the vapor pressure of C_6H_5OH is 1.67 Torr at this temperature.[31] The partial pressure of C_6H_5OH in the chamber was ~0.080 Torr. He (Scott Specialty Gases, 99.999%), in a minimal amount (~0.080 Torr), was added near the entrance port for the photolysis beam to suppress formation of a solid deposit on the quartz window. C_6H_5OH (Aldrich, 99%) was used without purification except for degassing; no impurity was detected in its IR spectrum.

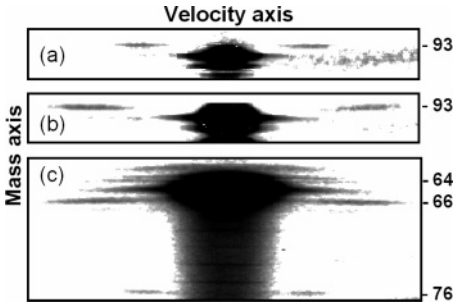

Figure 1. Images of photofragment ions upon photodissociation of phenol at 193 nm. The delays between pump and probe laser pulses are (a) 49, (b) 81, and (c) 10 μs.

3. Results

A. Photofragments and Translational Energy Distributions at 193 nm. Figure 1 depicts the photofragment ion images obtained upon photodissociation of phenol at 193 nm. Fragments with $m/z = 93$, 76, 66, 65, 64, and 63 were observed; images with $m/z = 94$, 95, and 96 correspond to phenol and its ^{13}C isotopes in natural abundance. The power dependence of the photolysis laser in the range of 0.43−3.43 mJ cm^{-2} showed that fragments with $m/z = 63$ and 64 were produced via two-photon dissociation, whereas all other fragments were from one-photon dissociation. Fragments resulting from multiphoton dissociation are not discussed here.

The image for $m/z = 93$ corresponds to the phenoxyl radical. The images at two delay intervals between pump and probe laser pulses are shown in Figure 1a and b. As the interval between pump and probe laser pulses was increased, the length of the image increased rapidly. This observation indicates that phenoxyl radicals are produced from the dissociation of excited phenol via elimination of a H atom. Both fragments with $m/z = 76$ and 66, corresponding to elimination of H_2O and CO molecules, respectively, have images of linear shape.

The image of the fragment with $m/z = 65$ possesses two components. A linearly shaped component is superimposed on a disk-like component at the center; the latter component resulted from the dissociative ionization of a heavier fragment by VUV photoionization because of the small ionization threshold of this fragment. There are only three possible fragments, $m/z = 93$, 76 and 66, which are heavier than $m/z = 65$. The fragment with $m/z = 76$ cannot crack into one with $m/z = 65$ because the difference of these two masses matches no observed or conceivable masses of atoms or molecules. Because the mass difference is small, fragment cracking from one with $m/z = 66$ into another with $m/z = 65$ would have insufficient recoil velocity to produce such a large disk-like image. As a result, the most likely fragment to generate the disk-like image has $m/z = 93$; the image at the center spreading from $m/z = 93$ to 65 represents the dissociation of an ion with $m/z = 93$ into another with $m/z = 65$ during the flight in the mass spectrometer. The translational energy distribution of the H-elimination channel, illustrated in Figure 2a, has taken the disk-like image for $m/z = 65$ into account. The slow component in the distribution of translational energy in the H-elimination channel results from only the disk-like component for $m/z = 65$, but

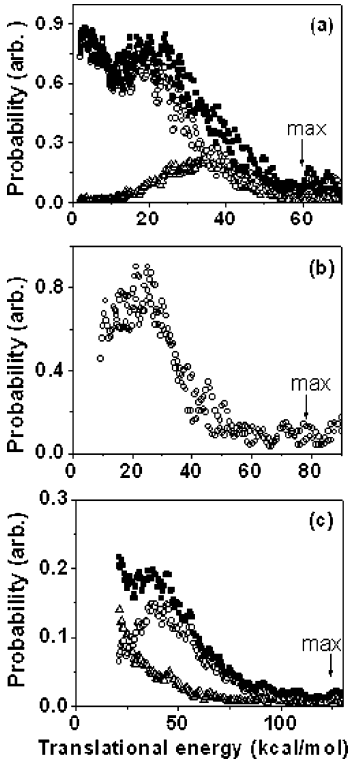

Figure 2. Distributions of translational energy for photofragments from (a) $C_6H_5OH + h\nu$ (193 nm) → $C_6H_5O + H$. Open triangles show the contribution from ions with $m/z = 93$, open circles show the contribution from the disk-like image for ions with $m/z = 65$, and solid squares denote the sum of these two, (b) $C_6H_5OH + h\nu$ (193 nm) → $C_6H_4 + H_2O$, and (c) $C_6H_5OH + h\nu$ (193 nm) → $C_5H_6 + CO$. Open circles show the contribution from ions with $m/z = 66$, open triangles are from the line shape image for ions with $m/z = 65$, and solid squares denote the sum of these two. Arrows indicate the maximum available energy.

the rapid component in the distribution of translational energy in the H-elimination channel results from ions with both $m/z = 65$ and 93.

The linearly shaped component with $m/z = 65$ corresponds to the fragment C_5H_5, but its corresponding fragmentation partner HCO was undetected. The translational energy (>30 kcal mol^{-1}) obtained from the image is greater than the available energy for the channel to produce $C_5H_5 + CO + H$. The most likely explanation is that it results from dissociative ionization of the central image corresponding to an ion with $m/z = 66$; that is, C_5H_6 with large internal energy. Unlike the disk-like image from other fragments, the image of $m/z = 65$ is linear because of the large mass ratio between C_5H_5 and H. We cannot exclude the possibility of a three-body dissociation channel to form $C_5H_5 + CO + H$, which has a small translational energy located at the central part of the linearly shaped image for an ion with $m/z = 65$.

The translational energy distributions for photofragments in various channels are shown in Figure 2. Except for the slow component in the H elimination (Figure 2a), all distributions of translational energy show a large release of translational energy. The observed maximum translational energy almost attains the maximum available energy of each channel.

The photodissociation of phenol-1-^{13}C was also studied. For the channel involving elimination of CO, we observed only ^{13}CO but no ^{12}CO from phenol-1-^{13}C. This result indicates that carbon atoms of the aromatic ring do not exchange before dissociation occurs.

B. Photofragments and Translational Energy Distributions at 248 nm. The images of photofragment ions obtained upon irradiation of phenol at 248 nm are similar to those obtained at 193 nm, as shown in Figure 3. Fragments with $m/z = 93$, 76, 66, and 65 were observed, but only ions with $m/z = 93$ and 66 and a disk-like component for $m/z = 65$ were from one-photon dissociation. At this wavelength, elimination of H_2O was unobserved in the one-photon process. The proportion of fragments with $m/z = 93$ cracking into the disk-like image with $m/z = 65$ due to dissociative ionization is much smaller than that observed at 193 nm. The distributions of translational energy of these dissociation channels are shown in Figure 4.

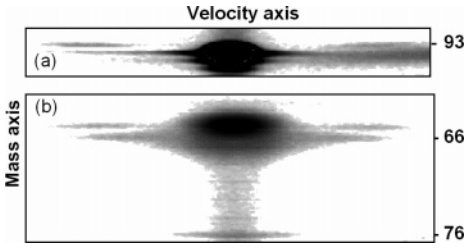

Figure 3. Images of photofragment ions upon the photodissociation of phenol at 248 nm. The delays between pump and probe laser pulses are (a) 95 and (b) 10 μs.

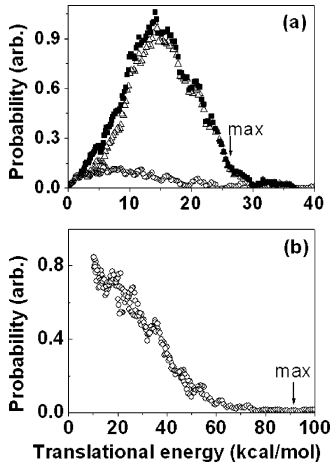

Figure 4. Distribution of translational energy for photofragments from (a) $C_6H_5OH + h\nu$ (248 nm) → $C_6H_5O + H$. Open triangles denote the contribution from ions with $m/z = 93$, open circles are from the disk-like image of ions with $m/z = 65$, and solid squares denote the sum of these two, (b) $C_6H_5OH + h\nu$ (248 nm) → $C_5H_6 + CO$. Arrows indicate the maximum available energy.

C. Infrared Emission of CO at 193 nm. In TR-FTS experiments, to approach a nearly collisionless condition within a 1.0 μs period, we decreased the partial pressures of C_6H_5OH (0.080 Torr) and He (0.080 Torr) as much as practicable while maintaining a satisfactory ratio of signal-to-noise. C_6H_5OH has an absorption cross section of $\sim 3.8 \times 10^{-17}$ cm^2 at 193 nm.[32] An investigation of the dependence of signal intensity on the fluence of the photolysis laser indicates that the signal intensity deviates from linearity when the laser fluence exceeds 30 mJ cm^{-2}. To determine the internal energy of CO, we hence performed experiments only with a photolysis fluence less than 30 mJ cm^{-2}.

Figure 5 shows partial emission spectra of CO, at a resolution of 0.3 cm^{-1}, recorded 0.2−1.2 and 1.2−2.2 μs after photolysis of C_6H_5OH in He. Vibration−rotational assignments were made based on spectral parameters reported by Ogilvie et al.[33] The spectrum exhibits emission from CO with J up to 70 and v up to 4. Each line in the R branch was normalized with the instrument response function and divided by its respective Einstein coefficient[34] to yield a relative population $P_v(J)$. Partially overlapped lines were deconvoluted to yield their

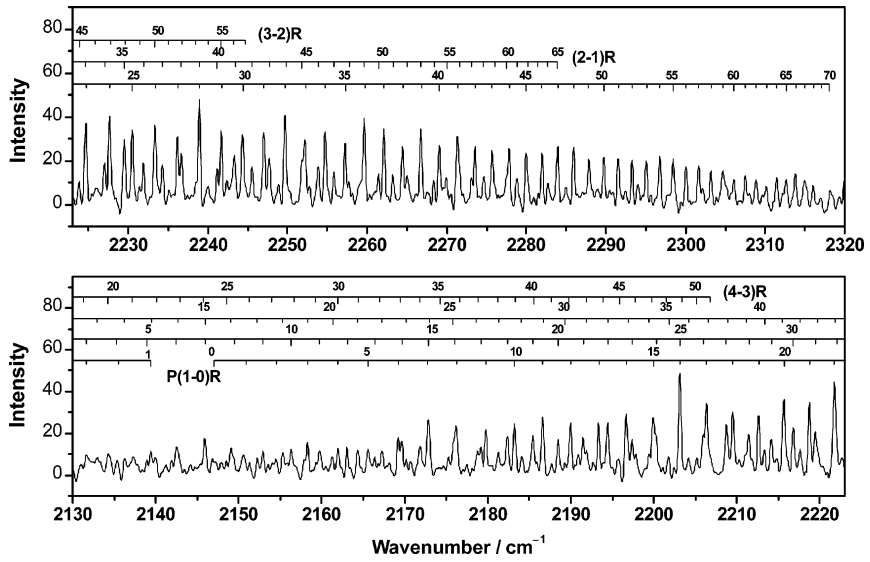

Figure 5. Infrared emission spectra of CO in spectral region of 2130−2320 cm^{-1} recorded 0.2−1.2 μs after photolysis of C_6H_5OH (0.080 Torr) in He (0.080 Torr) at 193 nm. The spectral resolution is 0.3 cm^{-1}; 27 laser pulses were averaged at each scan step of the interferometer, and three spectra recorded under similar experimental conditions were averaged. Assignments are shown as stick diagrams.

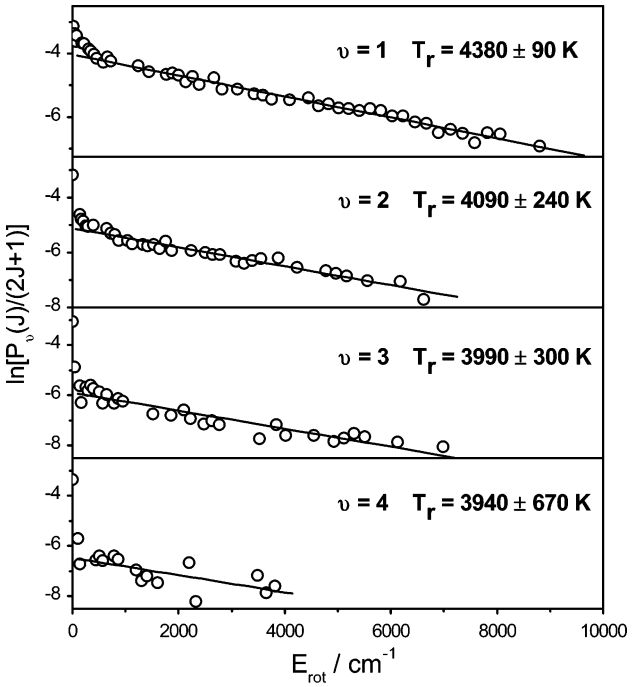

Figure 6. Semilogarithmic plots of relative rotational populations of CO ($v = 1-4$) upon photolysis of C_6H_5OH (0.080 Torr) in He (0.080 Torr) at 193 nm. Solid lines represent least-squares fits; data for small J values were excluded from the fitting because of interference due to quenching.

intensities. Semilogarithmic plots of $P_v(J)/(2J + 1)$ versus the rotational energy for CO ($v = 1-4$) recorded 0.2−1.2 μs after photolysis of C_6H_5OH are shown in Figure 6. Slightly enhanced populations at small J values are likely due to quenching and were excluded from the fitting. Fitted Boltzmann-like rotational distributions of CO, derived from the spectrum recorded in the range of 0.2−1.2 μs, yielded rotational temperatures of 4380 ± 90, 4090 ± 240, 3990 ± 300, and 3940 ± 670 K for $v = 1-4$, respectively; unless specified, listed error limits represent one standard deviation in fitting. The average rotational energy $E_r = 6.4$ kcal mol^{-1} for CO ($v = 1-4$) observed 0.2−1.2 μs after photolysis was derived. Similar procedures were undertaken for spectra averaged over 1.2−2.2, 2.2−3.2, and 3.2−4.2 μs. With a short extrapolation, we estimate the nascent rotational temperature to be 4610 ± 60 and 4450 ± 90 K for $v = 1$ and 2, respectively. After applying a correction factor of 1.07 (average of 4610/4380 = 1.05 and 4450/4090 = 1.09) for rotational quenching, we derived a nascent rotational energy of 6.9 ± 0.7 kcal mol^{-1}; the listed uncertainty represents an estimated error after considering the quenching effects.

We assumed a Boltzmann rotational distribution and associated an interpolated population for overlapped lines. Relative populations obtained on counting levels up to the observed J_{max} in each vibrational level were normalized to yield relative vibrational populations ($v = 1$)/($v = 2$)/($v = 3$)/($v = 4$) = (64.3 ± 0.5)/(22.2 ± 0.3)/(9.1 ± 0.4)/(4.4 ± 0.5), which correspond to a vibrational temperature of 3350 ± 30 K. Assuming a Boltzmann distribution, we estimate the population of $v = 0$ relative to $v = 1$ to be 2.26. The vibrational distribution of CO normalized for $v = 0-4$ is thus ($v = 0$)/($v = 1$)/($v = 2$)/($v = 3$)/($v = 4$) = 59.2/26.2/9.1/3.7/1.8. The average vibrational energy of CO thus derived is $E_v = 3.8$ kcal mol^{-1}. Considering errors in estimating the population of $v = 1$, we report E_v = 3.8 ± 0.7 kcal mol^{-1}.

4. Discussion

A. Dissociative Channels. The results of the experiments are describable according to the following reactions

$$C_6H_5OH + h\nu\ (193 \text{ or } 248 \text{ nm}) \rightarrow C_6H_5O + H$$

$$C_6H_5OH + h\nu\ (193 \text{ or } 248 \text{ nm}) \rightarrow C_5H_6 + CO$$

$$C_6H_5OH + h\nu\ (193 \text{ nm}) \rightarrow C_6H_4 + H_2O$$

Although a small contribution of the following reaction cannot be positively ruled out experimentally, theoretical calculations suggest that the contribution of this channel is small (see below).

$$C_6H_5OH + h\nu\ (193 \text{ nm}) \rightarrow C_5H_5 + HCO \rightarrow C_5H_5 + H + CO$$

The UV irradiation of phenol at 248 and 193 nm is expected to excite phenol to its S_1 and S_2 (or S_3) states, respectively. As these states are stable, dissociation must occur through the

coupling of these bound states with a repulsive state or via internal conversion or intersystem crossing to a lower electronic state, followed by dissociation. For the H-elimination channel, previous quantum chemical calculations show that an excited singlet state of $\pi\sigma^*$ character, which is repulsive with respect to the stretching of the OH bond, intersects both the S_1 and S_2 states.[16−18] H elimination at 248 nm was interpreted as involving predissociation via this repulsive state.[19] H elimination upon excitation at 193 nm might also be interpreted as a dissociation via the $\pi\sigma^*$ state through a coupling between S_2 and $\pi\sigma^*$ or through a coupling between S_1 and $\pi\sigma^*$ after internal conversion from S_2 to S_1. The fast component in the distribution of translational energy observed in the H-elimination channel must correspond to dissociation via this repulsive $\pi\sigma^*$ state. Although dissociation through the triplet state has been suggested[21,22] and the triplet potential energy surface correlating to dissociation products $H + C_6H_5O$ might have an exit barrier leading to a large translational energy release,[35,36] the dependence of the quantum yield on intersystem crossing and the independence of the quantum yield on dissociation on solvents indicate that dissociation of phenol in solution does not occur in the triplet state.[1] Furthermore, from studies of photodissociation of phenol at 193 nm in a condensed phase with Fourier-transform electron paramagnetic resonance and transient absorption spectra, the results indicate that the triplet state is not involved in the dissociative process.[2]

The slow component in the translational energy distribution of the H-elimination channel must correspond to dissociation from the ground state. The proportion of the slow component that increases as the excitation varies from 248 to 193 nm indicates the importance of H elimination from the electronic ground state at shorter UV wavelengths. Perhaps the rate of internal conversion to the ground state becomes very large at a short UV wavelength. The analogous phenomena with a large yield of internal conversion to the ground state upon excitation at 193 nm, in contrast to the large yield of internal conversion and/or intersystem crossing to the other electronic excited state upon excitation at 248 nm, have been observed in similar systems such as ethylbenzene and propylbenzene.[35,36]

The mechanisms for dissociation into CO and H_2O differ from that for elimination of a H atom. The average translational energies in the CO-elimination and H_2O-elimination channels are large. The observed maximum translational energy nearly attains the maximum available energy for both channels. The difference between the observed maximum translational energy and the maximum available energy is smaller than the energies of the electronically excited states of these fragments. As a result, fragments of both channels, $C_5H_6 + CO$ and $C_6H_4 + H_2O$, were produced in their electronic ground states. As the ground state of these closed-shell fragments correlates only with the ground state of the parent molecule, the dissociation must occur on the ground electronic surface.

B. Potential-Energy Surface and Branching Ratios from Calculations. Table 1 lists the vertical excitation energies of phenol for the singlet and triplet states, calculated with time-dependent density functional theory (TD-B3LYP)[37] using Gaussian 03[38] and complete active space second-order perturbation theory (CASPT2)[39] using MOLPRO[40] with the 6-311G(d,p) basis set. Eight active orbitals and eight active electrons were specified in the CASPT2 calculation. Comparison with experimental data[41−45] indicates that the excited singlet energies predicted with CASPT2 are better than those with TD-B3LYP, particularly in the first excited state S_1; the errors in predicted energy of S_1 are −3.1 kcal mol^{-1} at CASPT2 and 14.6 kcal mol^{-1} at TD-B3LYP. According to Figure 7, we predict that light at 248 nm is able to excite a phenol molecule from the ground state to the first exited state S_1 for the isomerization and decomposition reactions to proceed. Apparently because of the spin-forbidden nature of the transition from S_0 to T_1, the reaction seems not to occur in the triplet excited state, despite the energies of the first three triplet states being less than those of photons corresponding to laser lines at 248 or 193 nm.

TABLE 1: Vertical Excitation Energies of Phenol in Both Singlet and Triplet States (in Units of kcal mol^{-1})

	TD-B3LYP	CASPT2	exptl data
S_0	0	0	0
S_1	118.5	100.8	103.9[a]
			104.0[b]
S_2	138.1	142.4	133.1[b]
			137.9[c]
S_3	138.9	147.9	153.6[b]
T_1	80.3	86.3	
T_2	109.5	98.9	
T_3	121.6	103.9	
T_4	138.3	134.5	

[a] Refs 41−43. [b] Ref 44. [c] Ref 45.

Various dissociation channels of phenol in its ground electronic surface have already been calculated with the G2M//B3LYP/6-311G(d,p) method.[46] Figure 7 shows a simplified potential energy diagram for these channels. Most structures of intermediates (M1−M8) and transition states (TS1−TS15) except those (M9, M10, TS16, and TS17) involving the $C_5H_5 + HCO$ channel have been published in this previous study;[46] they are given in the Supporting Information. If we neglect contributions of the channels via transition states TS1, TS9, TS10, TS16, and TS17 due to their higher barriers, the accessible paths are describable as follows

$$C_6H_5OH \rightarrow C_6H_5O + H \quad (1a)$$

$$C_6H_5OH \xrightarrow{TS3} M1 \rightarrow C_6H_5O + H \quad (1b)$$

$$C_6H_5OH \xrightarrow{TS3} M1 \xrightarrow{TS6} M3 \xrightarrow{TS13} M7 \xrightarrow{TS14} C_5H_6 + CO \quad (2a)$$

$$C_6H_5OH \xrightarrow{TS3} M1 \xrightarrow{TS6} M3 \xrightarrow{TS13} M7 \xrightarrow{TS15} C_5H_6 + CO \quad (2b)$$

$$C_6H_5OH \xrightarrow{TS3} M1 \xrightarrow{TS4} M2 \xrightarrow{TS5} C_5H_6 + CO \quad (2c)$$

$$C_6H_5OH \xrightarrow{TS2} C_6H_4 + H_2O \quad (3)$$

Direct dissociation of phenol to form $C_6H_5O + H$, reaction 1a, requires 89.1 kcal mol^{-1}. The H atom might migrate from the OH group to form *ortho*- cyclohexadienone (M1), followed by H elimination, reaction 1b. The CO elimination might proceed via several dissociative pathways; the most feasible pathway, reaction 2a, begins with migration of the H atom from the OH group to form M1, followed by further H-atom migration along the six-membered ring to form *meta*-cyclohexadienone (M3); M3 then isomerizes to a bicyclic isomer (M7) before decomposition into *cyclo*-$C_5H_6 + CO$ via TS14. Although this path includes three intermediates and four transition states, the largest barrier height is only 75.8 kcal mol^{-1}. Reaction 2b proceeds similarly to reaction 2a except for the last step, in which M7 decomposes via TS15 with a barrier height of 84.0 kcal mol^{-1}. The third channel, reaction 2c, has a barrier height of 86.1 kcal mol^{-1}. In principle, CO can also be produced from

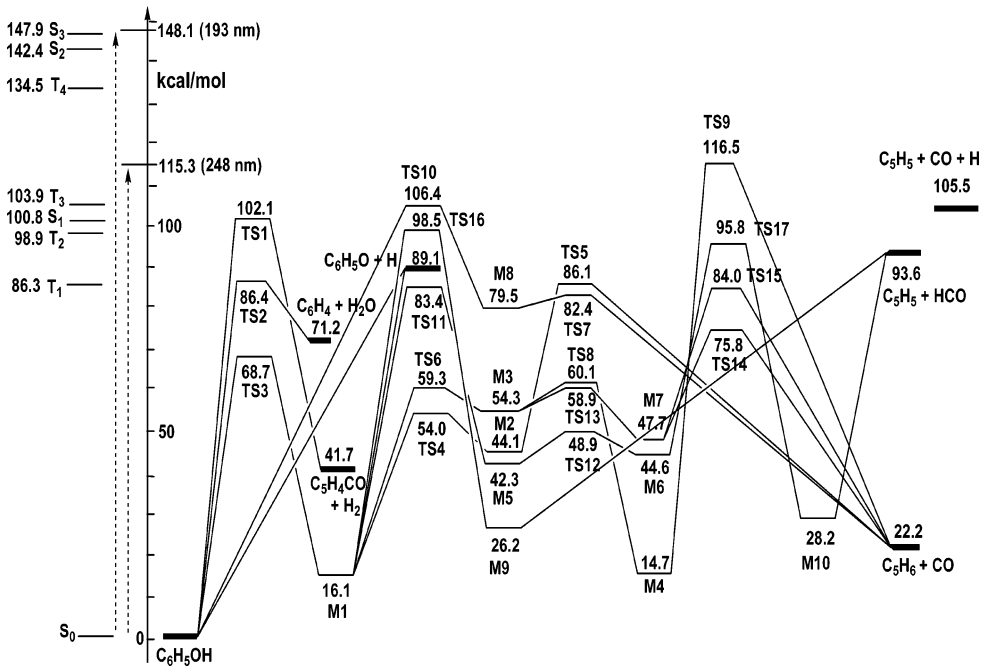

Figure 7. Schematic diagram of the energy for isomerization and dissociation reactions of C_6H_5OH at the G2M//B3LYP/6-311G(d,p) level of theory and the excited energy levels of C_6H_5OH at the CASPT2 level of theory.

fragmentation of the internally excited C_6H_5O formed in reactions 1a and 1b. The theoretical barrier for the fragmentation of C_6H_5O to give $C_5H_5 + CO$ has been computed at the G2M level of theory to be 52 kcal mol^{-1} with a very tight transition state.[47] The total barrier for the formation of $C_5H_5 + H + CO$ is 141 kcal mol^{-1}, which is almost twice that of TS14. Accordingly, the contribution of this route to CO should be negligible. The channel to eliminate H_2O, reaction 3, proceeds via the four-center elimination via TS2 with a barrier height of 86.4 kcal mol^{-1}. Elimination of HCO is predicted to occur through TS16 and M9 from M1 and through TS17 and M10 from M6. The barriers for these two channels are 98.5 and 95.8 kcal mol^{-1}, respectively, which are greater than that of the CO-elimination pathway by about 20 kcal mol^{-1}. In the isomerization and decomposition from M1, elimination of CO is hence most favorable. Although phenol can isomerize to a seven-membered ring isomer (M6) with a barrier of only 83.4 kcal mol^{-1}, our experiment on phenol-1-^{13}C shows that this isomerization is unimportant in CO elimination under our experimental conditions.

To elucidate the contribution of each product channel of $C_5H_6 + CO$, $C_6H_5O + H$, and $C_6H_4 + H_2O$ upon excitation of phenol at 193 and 248 nm, we calculated the microcanonical rate coefficients $k(E)$ over a wide range of energies with the microcanonical RRKM theory and the stationary-state treatment to the multiwell product channels. The rate coefficients and branching ratios for these three product channels as a function of energy are plotted in Figure 8. The curve of $k_{CO}(E)$ intersects $k_H(E)$ and $k_{H_2O}(E)$ at ~120 and 200 kcal mol^{-1}, respectively. The major products are hence predicted to be $C_5H_6 + CO$ at energies under 120 kcal mol^{-1} and $C_6H_5O + H$ for $E > 120$ kcal mol^{-1}. At 248 nm ($E = 115$ kcal mol^{-1}), the predicted values of $k_{CO}(E)$, $k_H(E)$, and $k_{H2O}(E)$ are 1.7×10^5, 1.5×10^5, and 1.4×10^3 s^{-1}, respectively, with $k_{CO}(E)$ being slightly greater than $k_H(E)$. In contrast, $k_{CO}(E)$, $k_H(E)$, and $k_{H2O}(E)$ are 1.1×10^7, 2.2×10^8, and 1.0×10^6 s^{-1}, respectively, at 193 nm ($E = 148$ kcal mol^{-1}), with $k_{CO}(E)$ being less than one twentieth of $k_H(E)$. Although $k_{H_2O}(E)$ is the smallest for the three product channels, it might attain the observable value at 193 nm. These theoretically predicted rates are in satisfactory agreement with the large fragment ion intensities of $m/e = 93$, 66, and 65 in our experimental measurements.

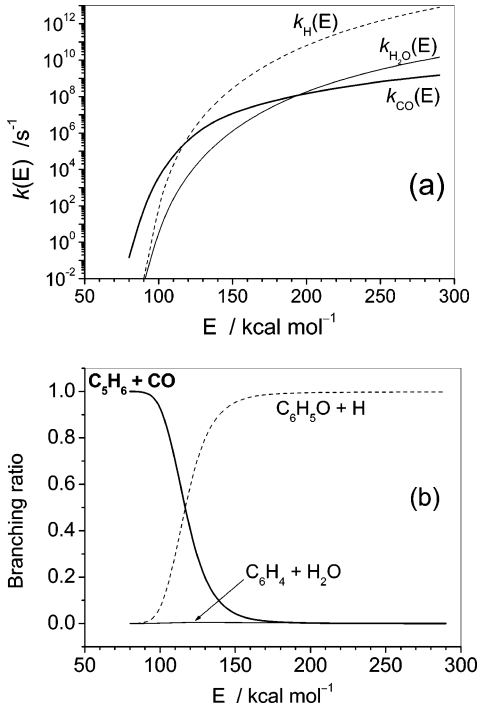

Figure 8. (a) Microcanonical rate coefficients versus energy for production of $C_5H_6 + CO$, $C_6H_5O + H$, and $C_6H_4 + H_2O$ on the singlet potential energy surface. (b) Branching ratios of individual products versus energy.

The branching ratios for various paths in product channels $C_5H_6 + CO$ and $C_6H_5O + H$ are shown in Figure 9a and b, respectively. In Figure 9a, reaction 2a is preponderant among the three channels of the products $C_5H_6 + CO$ upon photolysis at 193 nm because of its small barrier (75.8 kcal mol^{-1}) associated with TS14; its branching ratio decreases with increasing energy and equals the branching ratio for channel 2c at 260 kcal mol^{-1}. Channel 2b has the smallest branching

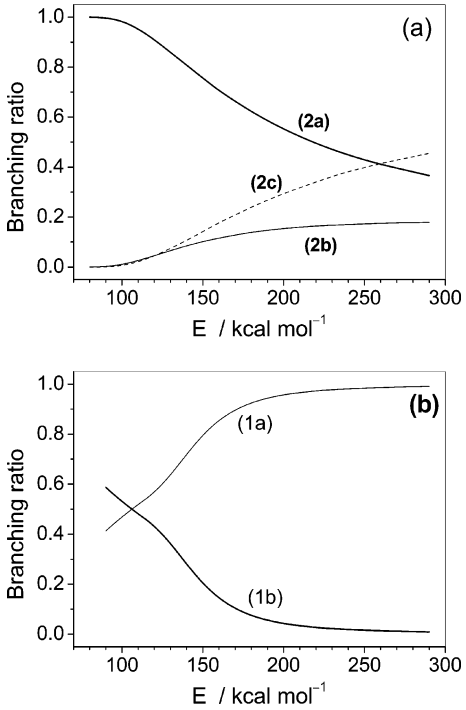

Figure 9. (a) Branching ratios of channels 2a, 2b, and 2c relative to the total rate of CO production. (b) Branching ratios of channels 1a and 1b relative to the total rate of H production from the electronic ground state.

ratio throughout the calculated energy range. The branching ratios of the channels 2a, 2b, and 2c are 0.93, 0.04, and 0.03, respectively, at 248 nm and 0.76, 0.10, and 0.13 at 193 nm. Notice that the RRKM calculation only takes the dissociation channels in the ground state into account. The H-atom elimination from the excited state is not taken into consideration.

For the H-elimination channel, the point of intersection of the branching ratios of channels 1a and 1b is about 105 kcal mol^{-1}, as shown in Figure 9b, with reaction 1b dominating at smaller energies. At ~250 kcal mol^{-1}, the branching ratio of reaction 1a approaches unity. The branching ratios of the channels 1a and 1b are 0.55 and 0.45, respectively, at 248 nm and 0.78 and 0.22 at 193 nm.

C. Distribution of CO States. Reaction 2a is predicted to be the major channel upon photolysis of phenol at 193 nm; it proceeds via TS14 before the CO molecule is eliminated. The observed average translational energy for the CO-elimination channel is ~45 kcal mol^{-1}, consistent with the exit barrier of 53.6 kcal mol^{-1} calculated for reaction 2a. The internal energy of the two photofragments is hence ~81 kcal mol^{-1}; only 10.6 kcal mol^{-1} goes to CO. This is conceivable because the other fragment C_5H_6 is more complex. In preceding work, we employed a revised impulse model to satisfactorily explain the rotational energy of HX (X = F, Cl, and Br) produced upon photolysis of halocompounds at 193 nm via four-center elimination.[30,48−50] For reaction 2a, TS14 undergoes a simple bond rupture to form CO and C_5H_6. We employed a modified impulse model for fragmentation of a triatomic molecule[51] to predict the rotational energy of CO to be 5.5 kcal mol^{-1} according to the bond angle of 167° of TS14 and the available energy of 53.6 kcal mol^{-1}. Similarly, rotational energies of 8.7 and 28.7 kcal mol^{-1} are predicted for reactions 2b and 2c, respectively, with available energies and angles of 61.8 kcal mol^{-1} and 164.5° and 63.9 kcal mol^{-1} and 143.3°. Using the branching ratios of 0.76, 0.10, and 0.13 for channels 2a, 2b, and 2c, an average rotational energy of 8.8 kcal mol^{-1} is derived. If only reactions 2a and 2b are taken into account, an average rotational energy of 5.9 kcal mol^{-1} is derived, consistent with the observed rotational energy of 6.9 kcal mol^{-1}.

The partition of vibrational energy depends on the deviation of the distance between two bond-forming atoms from the equilibrium bond length. The predicted distance between C and O atoms for TS14 in the dissociation of C_6H_5OH is 1.163 Å. Because the equilibrium bond distance of CO is 1.128 Å,[52] the vibrational excitation of CO is expected to be small. For comparison, HF produced via the four-center elimination of CH_2CHF has greater vibrational energy (20 ± 2 kcal mol^{-1})[49] than that (11.5 ± 1.4 kcal mol^{-1})[50] from CF_2CHCl because the predicted bond distances in the transition structures are 1.28 and 1.18 Å, respectively, and that of HF is 0.917 Å.[53] The small vibrational energy of product CO due to the late-barrier character of the transition structure is consistent with the large release of translational energy in our measurement. If the available energies above all three low-lying transition states (TS5, TS14, and TS15) leading to the C_5H_6 + CO products are statistically distributed, one can estimate the CO vibrational energy distribution by using the predicted specific rate coefficients, $k_i[E_i - E_i(\upsilon)]$, in which E_i and $E_i(\upsilon)$ represent the available energy and the CO vibrational energy at its υth level, respectively. Using the branching ratios for the three channels (2a, 2b, and 2c) given above, we get ($\upsilon = 0$)/($\upsilon = 1$)/($\upsilon = 2$)/($\upsilon = 3$)/($\upsilon = 4$)/($\upsilon = 5$) = 39.5/26.1/16.2/9.9/5.5/2.8. The distribution is noticeably hotter than the experimental result 59.2/26.2/9.1/3.7/1.8. Part of the deviation might be due to the colder CO vibrational distributions from several triple product fragmentation reactions giving C_5H_5 + H + CO.

5. Conclusion

The major dissociation channels for phenol at 193 nm include OH bond fission, CO elimination, and H_2O elimination. Only the former two channels are observed at 248 nm. The translational energy distribution indicates that H-atom elimination occurs in both the electronically excited and ground states, but elimination of CO or H_2O occurs in the electronic ground state. Upon photolysis of phenol at 193 nm, CO ($v \leq 4$) shows a nascent rotational temperature of ~4600 K and a vibrational temperature of ~3350 K; a relatively small fraction of available energy goes to the internal energy of CO. The dissociation channels, the translational energy distributions of the photofragment, and the internal energy of product CO are consistent with potential energy surfaces from quantum chemical calculations and the branching ratios from an RRKM calculation.

Acknowledgment. National Science Council, Taiwan, supported this work under Contracts NSC93-2113-M-001-007 and NSC95-2119-M-009-032. Z.F.X. thanks the DOE Basic Energy Sciences for a partial support of this work. M.C.L. is grateful to the National Science Council of Taiwan for the Distinguished Visiting Professorship and the Taiwan Semiconductor Manufacturing Co. for the TSMC Distinguished Professorship at the National Chiao Tung University, Taiwan.

Supporting Information Available: Figures of geometries of all local minima (M1−M10) and transition states (TS1−TS17) together with tables of structures and rotational moments of inertia and harmonic frequencies of all species optimized at the B3LYP/6-311G** level of theory. This material is available free of charge via the Internet at http://pubs.acs.org.

References and Notes

(1) Hermann, R.; Mahalaxmi, G. R.; Jochum, T.; Naumov, S.; Brede, O. *J. Phys. Chem. A* **2002**, *106*, 2379.
(2) Bussandri, A.; Willigen, H. *J. Phys. Chem. A* **2002**, *106*, 1524.
(3) Solgadi, C.; Jouvet, D.; Tramer, A. A. *J. Phys. Chem.* **1988**, *92*, 3313.
(4) Jouvet, C.; Dedonder-Lardeux, C.; Richard-Viard, M.; Solgadi, D.; Tramer, A. *J. Phys. Chem.* **1990**, *94*, 5041.
(5) Steadman, J.; Syage, J. A. *J. Phys. Chem*. **1990**, *92*, 4630.
(6) Syage, J. A.; Steadman, J. *J. Chem. Phys*. **1991**, *95*, 2497.
(7) Steadman, J.; Syage, J. A. *J. Am. Chem. Soc.* **1991**, *113*, 6786.
(8) Syage, J. A.; Steadman, J. *J. Phys. Chem*. **1992**, *96*, 9606.
(9) Syage, J. A. *Chem. Phys. Lett.* **1993**, *202*, 227.
(10) Hineman, M. F.; Kelley, D. F.; Bernstein, E. R. *J. Chem. Phys*. **1993**, *99*, 4533.
(11) Jacoby, C.; Hering, P.; Schmitt, M.; Roth, W.; Kleinermanns, K. *Chem. Phys.* **1998**, *23*, 239.
(12) Pino, G.; Grégoire, G.; Dedonder-Lardeux, C.; Jouvet, C.; Martrenchard, S.; Solgadi, D. *J. Chem. Phys.* **1999**, *111*, 10747.
(13) Pino, G.; Grégoire, G.; Dedonder-Lardeux, C.; Jouvet, C.; Martrenchard, S.; Solgadi, D. *Phys. Chem. Chem. Phys.* **2000**, *2*, 893.
(14) Ishiuchi, S.; Saeki, M.; Fujii, M. *Chem. Phys. Lett.* **2000**, *322*, 27.
(15) Ishiuchi, S.; Saeki, M.; Daigoku, K.; Ueda, T.; Yamanaka, T.; Hashimoto, K.; Fujii, M. *Chem. Phys. Lett.* **2001**, *347*, 87.
(16) Sobolewski, A. L.; Domcke, W. *J. Phys. Chem. A* **2001**, *105*, 9275.
(17) Sobolewski, A. L.; Domcke, W.; Dedonder-Lardeux, C.; Jouvet, C. *Phys. Chem. Chem. Phys.* **2002**, *4*, 1093.
(18) Daigoku, K.; Ishiuchi, S.; Sakai, M.; Fujii, M.; Hashimoto, K. *J. Chem. Phys.* **2003**, *119*, 5149.
(19) Tseng, C. M.; Lee, Y. T.; Ni, C. K. *J. Chem. Phys.* **2004**, *121*, 2459.
(20) Nix, M. G. D.; Devine, A. L.; Cronin, B.; Dixon, R. N.; Ashfold, M. N. R. *J. Chem. Phys.* **2006**, *125*, 133318.
(21) Dellonte, S.; Marconi, G. *J. Photochem.* **1985**, *30*, 37.
(22) Dellonte, S.; Marconi, G.; Monti, S. *J. Photochem.* **1987**, *39*, 33.
(23) Schick, C. P.; Carpenter, S. D.; Weber, P. M. *J. Phys. Chem. A* **1999**, *103*, 10470.
(24) Kaji, Y.; Obi, K.; Nakashima, N.; Yoshihara, K. *J. Chem. Phys*. **1987**, *87*, 5059.
(25) Tsai, S. T.; Lin, C. K.; Lee, Y. T.; Ni, C. K. *Rev. Sci. Instrum.* **2001**, *72*, 1963.
(26) Tsai, S. T.; Lin, C. K.; Lee, Y. T.; Ni, C. K. *J. Chem. Phys.* **2000**, *113*, 67.
(27) Tsai, S. T.; Huang, C. L.; Lee, Y. T.; Ni, C. K. *J. Chem. Phys.* **2001**, *115*, 2449.
(28) Yeh, P.-S.; Leu, G.-H.; Lee, Y.-P.; Chen, I-C. *J. Chem. Phys.* **1995**, *103*, 4879.
(29) Lin, S.-R.; Lee, Y.-P. *J. Chem. Phys*. **1999**, *111*, 9233.
(30) Wu, C.-Y.; Wu, Y.-J.; Lee, Y.-P. *J. Chem. Phys.* **2004**, *121*, 8792.
(31) Dreisbach, R. R.; Shrader, S. A. *Ind. Eng. Chem*. **1949**, *41*, 2879.
(32) Martynoff, M. *Bull. Soc. Chim. Fr*. **1949**, *16*, 258.
(33) Ogilvie, J. F.; Cheah, S.-L.; Lee, Y.-P.; Sauer, S. P. A. *Theor. Chem. Acc.* **2002**, *108*, 85.
(34) Ogilvie, J. F. *The Vibrational and Rotational Spectrometry of Diatomic Molecules*; Academic Press: London, 1998.
(35) Huang, C. L.; Jiang, J. C.; Lin, S. H.; Lee, Y. T.; Ni, C. K. *J. Chem. Phys.* **2002**, *116*, 7779.
(36) Huang, C. L.; Jiang, J. C.; Lee, Y. T.; Ni, C. K. *J. Chem. Phys.* **2002**, *117*, 7034.
(37) Stratmann, R. E.; Scuseria, G. E.; Frisch, M. J. *J. Chem. Phys.* **1998**, *109*, 8218.
(38) Frisch, M. J.; Trucks, G. W.; Schlegel, H. B.; Scuseria, G. E.; Robb, M. A.; Cheeseman, J. R.; Montgomery, J. A., Jr.; Vreven, T.; Kudin, K. N.; Burant, J. C.; Millam, J. M.; Iyengar, S. S.; Tomasi, J.; Barone, V.; Mennucci, B.; Cossi, M.; Scalmani, G.; Rega, N.; Petersson, G. A.; Nakatsuji, H.; Hada, M.; Ehara, M.; Toyota, K.; Fukuda, R.; Hasegawa, J.; Ishida, M.; Nakajima, T.; Honda, Y.; Kitao, O.; Nakai, H.; Klene, M.; Li, X.; Knox, J. E.; Hratchian, H. P.; Cross, J. B.; Bakken, V.; Adamo, C.; Jaramillo, J.; Gomperts, R.; Stratmann, R. E.; Yazyev, O.; Austin, A. J.; Cammi, R.; Pomelli, C.; Ochterski, J. W.; Ayala, P. Y.; Morokuma, K.; Voth, G. A.; Salvador, P.; Dannenberg, J. J.; Zakrzewski, V. G.; Dapprich, S.; Daniels, A. D.; Strain, M. C.; Farkas, O.; Malick, D. K.; Rabuck, A. D.; Raghavachari, K.; Foresman, J. B.; Ortiz, J. V.; Cui, Q.; Baboul, A. G.; Clifford, S.; Cioslowski, J.; Stefanov, B. B.; Liu, G.; Liashenko, A.; Piskorz, P.; Komaromi, I.; Martin, R. L.; Fox, D. J.; Keith, T.; Al-Laham, M. A.; Peng, C. Y.; Nanayakkara, A.; Challacombe, M.; Gill, P. M. W.; Johnson, B.; Chen, W.; Wong, M. W.; Gonzalez, C.; Pople, J. A. *Gaussian 03*, revision C.02; Gaussian, Inc.: Wallingford, CT, 2004.
(39) Celani, B. P.; Werner, H.-J. *J. Chem. Phys.* **2000**, *112*, 5546.
(40) Werner, H.-J.; Knowles, P. J.; Lindh, R.; Manby, F. R.; Schütz, M.; Celani, P.; Korona, T.; Rauhut, G.; Amos, R. D.; Bernhardsson, A.; Berning, A.; Cooper, D. L.; Deegan, A. J.; Dobbyn, F.; Eckert, C.; Hampel and G. Hetzer, A. W. Lloyd, S. J. McNicholas, M. J. O.; Meyer, W.; Mura, M. E.; Nicklass, A.; Palmieri, P.; Pitzer, R.; Schumann, U.; Stoll, H.; Stone, A. J.; Tarroni, R.; Thorsteinsson, T. *MOLPRO, version 2006.1, a package of ab initio programs*; see www.molpro.net.
(41) Lemaire, E. J.; Dimicoli, I.; Piuzzi, F.; Botter, D. R. *Chem. Phys.* **1987**, *115*, 119.
(42) Berden, G.; Meerts, W. L.; Schmitt, M.; Kleinermanns, K. *J. Chem. Phys.* **1995**, *104*, 972.
(43) Nix, M. G. D.; Devine, A. L.; Cronin, B.; Dixon, R. N.; Ashfold, M. N. R. *J. Chem. Phys.* **2006**, *125*, 133318.
(44) Lorentzon, J.; Malmqvist, P.-A.; Fiilscher, M.; Roos. B. O. *Theor. Chim. Acta* **1995**, *91*, 91.
(45) Schick, C. P.; Carpenter, S. D.; Weber, P. M. *J. Phys. Chem. A* **1999**, *103*, 10470.
(46) Xu, Z. F.; Lin, M. C. *J. Phys. Chem. A* **2006**, *110*, 1672.
(47) Liu, R.; Morokuma, K.; Mebel, A. M.; Lin, M. C. *J. Phys. Chem.* **1996**, *100*, 9314.
(48) Lin, S.-R.; Lin, S.-C.; Lee, Y.-C.; Chen, I-C.; Lee, Y.-P. *J. Chem. Phys.* **2001**, *114*, 160.
(49) Lin, S.-R.; Lin, S.-C.; Lee, Y.-C.; Chou, Y.-C.; Chen, I-C.; Lee, Y.-P. *J. Chem. Phys.* **2001**, *114*, 7396.
(50) Wu, C.-Y.; Chung, C.-Y.; Lee, Y.-C.; Lee, Y.-P. *J. Chem. Phys.* **2002**, *117*, 9785.
(51) Busch, G. E.; Wilson, K. R. *J. Chem. Phys.* **1972**, *56*, 3626.
(52) Bunker, P. R. *J. Mol. Spectrosc.* **1970**, *35*, 306.
(53) Huber, K. P.; Herzberg, G. *Constants of Diatomic Molecules*; van Nostrand: Princeton, NJ, 1979.